SPECTRAL CHARACTERISTICS OF 253.7 nm MERCURY LINE

A.B. Antipov, E.Yu. Genina, and D.O. Kuchmezov

Institute of Optical Monitoring,
Siberian Branch of the Russian Academy of Sciences, Tomsk,
D.I. Mendeleev Scientific Research Institute of Metrology, St. Petersburg
Received February 12, 1998

Radiation of mercury emission line at 253.7 nm *and its absorption is widely used in many spectroscopic, photochemical, analytical, and magnetometric tasks as well as in other scientific and engineering applications. Physical and chemical peculiarities of mercury as well as the demand to determine its microconcentrations (as small as the background level) made the mercury gas analyzers to be a separate class of analytical devices. In this paper we present the line parameters which one should take into account in applied investigations (line width, collision broadening and shift, Zeeman splitting, isotopic and hyperfine structure). The data from references are supplemented with the results obtained by the authors.*

GENERAL PROPERTIES

The resonance mercury line at $\lambda = 253.652$ nm is the $6^1S_0 - 6^3P_1$ intercombination. The term "resonance lineB means that atom returns to its ground state emitting a photon $h\nu$ of the same frequency ν as the absorbed one. The term structure of mercury atom was described in a number of papers (see, for example, Ref. 1).

The "resonance lineB term is usually applied to one or several lines that are most intense at a resonance emission. Transitions from the most deep excited levels to the ground one yield such lines. For mercury atom, resonance line is the line with the wavelength of 254 nm due to the transition from one of the sublevels of the first excited level $^3P_1$ which is a triple level (transitions from $^3P_2$ and $^3P_0$ sublevels are forbidden).

Transitions between terms of different multiplicity are called intercombination ones. The selection rule that forbids such transitions, holds more strictly for lighter atom. For heavy atoms, like mercury atom, the probability of such transitions is high enough.

Very high intensity of the 254-nm line can be explained by the fact that, although its transition probability is a bit less than for transitions without violation of the selection rule $\Delta S = 0$ and equals to 0.93 by 10^7 s^{-1} (lifetime, τ, is equal to 1.08 by 10^{-7} s), but the conditions of excitation are very favorable. Those result not only from direct excitation of the 6^3P_1 level with the energy of 4.89 eV, but from other excitation processes as well.

In parallel with the 6^3P_1 level metastable levels 6^3P_0 and 6^3P_2, with close excitation energies of 4.67 and 5.46 eV, of the same term are also directly excited in the electric gas discharge. The probability of nonradiative transitions from these levels to the ground state (6^1S_0) is low because under these conditions large energy, of the order of 5 eV, should be transferred to the kinetic form. So, at collisions the 6^3P_1 level is excited with a high probability because the transition from 6^3P_2 to the latter one is accompanied by release of 0.57 eV energy while the transition from 6^3P_0 by the consumption of 0.20 eV energy that comes from thermal energy due to collisions. The transitions from higher excited levels happen both to 6^3P_1 and 6^3P_0 and 6^3P_2, so the number of processes which contribute to the emission at 254-nm line is rather large.[1,2]

ISOTOPIC AND HYPERFINE STRUCTURE

Natural mercury occurs in the form of seven stable isotopes with atomic mass of 196, 198, 199, 200, 201, 202, and 204. The components of a spectral line corresponding to lighter isotopes are usually shifted toward higher frequency, including the case with 254-nm line, but the inverse situation may also occur, as, for example with the 607-nm mercury line.[1] The sign of a frequency shift depends on the relative shifts of the relevant terms. The odd isotope lines have a hyperfine structure with the width that is comparable to the isotopic split. The isotopic line shifts have been comprehensively studied in Refs. 1, 3, 5, and 6. Most detailed quantitative characteristics accounting hyperfine structure may be found in Ref. 3 and are presented in Fig. 1 and Table I.

The isotopic composition obtained by different authors is presented in Fig. 2. Ten lines of isotopic and hyperfine structure form five groups that are spaced by a distance about 3 times larger than Doppler width under normal conditions. Figures *1* to *5* in Fig. 2 denote centers of the line groups obtained in our experiment, letters Φ denote the data from Ref. 1, other data are from Ref. 3. We recorded the spectra on a UFSH–3 photoplate placed into a cassette of a diffraction

0235-6880/98/07 582-08 $02.00

spectrograph DFS–452 (the spectral resolution in the region near 200 nm was, according to Ref. 7, 120000) crossed with an IT–28–30 Fabry-Perot interferometer.

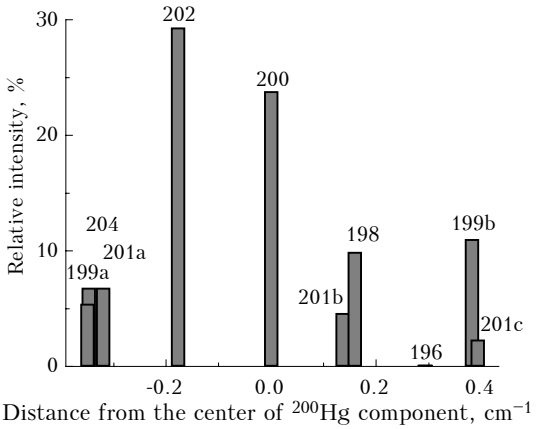

FIG. 1. Intensity distribution among the components of isotopic and hyperfine structure of 254-nm *mercury resonance line.*

TABLE I. Intensity distribution among the components of the isotopic and hyperfine structure of the mercury line at 254 nm.

Component	Radiation intensity, %	Relative shift, cm^{-1}
200	23.8	0
202	29.3	− 0.177
201a	6.8	− 0.320
204	6.8	− 0.348
199a	5.4	− 0.350
201b	4.6	0.136
198	9.9	0.159
196	0.146	0.293
199b	11.0	0.382
201c	2.3	0.393

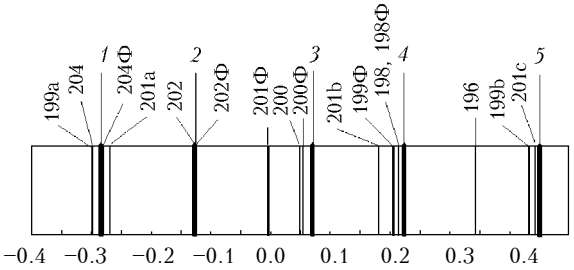

FIG. 2. Isotopic and hyperfine structure of 254-nm *mercury line reproduced from data by different authors.*

Parameters of the interferometer were determined using known expressions.[8,9] To make the choice of the interferometer base and reflection coefficients of mirrors easier, the main dependences of interferometer spectral characteristics are shown in Figs. 3 to 5.

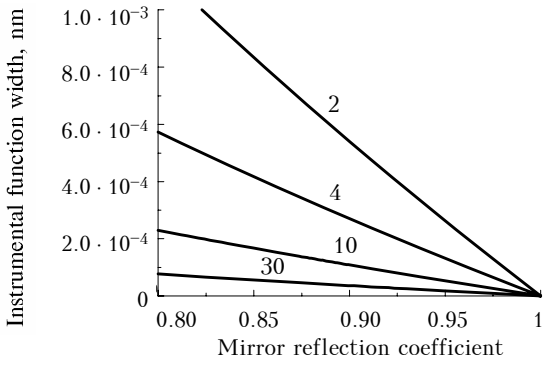

FIG. 3. Dependence of instrumental function width of a Fabry-Perot interferometer on plate separation and reflection coefficients of mirror.

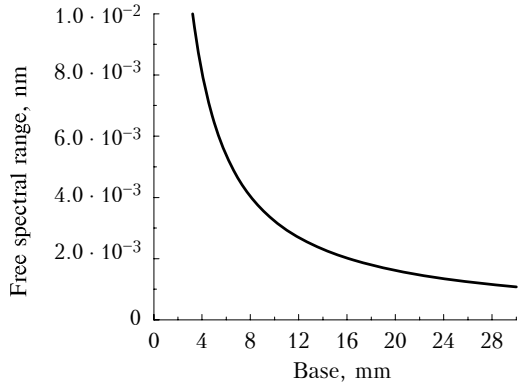

FIG. 4. Dependence of the free spectral range of a Fabry-Perot interferometer on plate separation for λ = 254 nm.

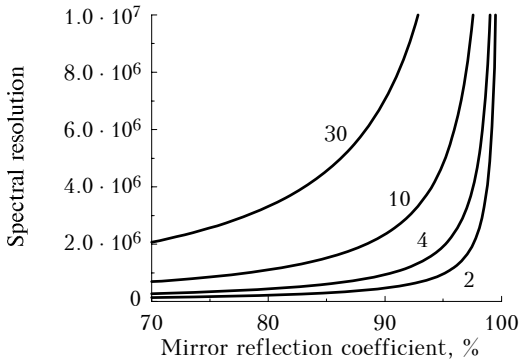

FIG. 5. Dependence of the Fabry-Perot interferometer spectral resolution on mirror reflection coefficients. The mirror reflection coefficients are thought to be equal, the transmittance of the gap between mirrors is equal to 100%. *The separation between mirrors is* 2, 4, 10, *and* 30 mm.

Preliminary work with the standard aluminum mirror coatings showed that their reflection coefficients (R = 0.8 at 250 nm for new coatings, then it decreases to 0.65) do not provide for an appropriate spectral resolution. Therefore we replaced the coatings for the

dielectric ones with the reflectivity of 0.95 at $\lambda = 254$ nm. In practice we obtained spectral resolution of 550000 and the ratio between the full width at half maximum (FWHM) of a separate line and free spectral range to be equal 1/10. The ratio of calculated Doppler line width, γ_D, and instrumental function width, $\delta\nu$, to the free spectral range, $\Delta\nu$, were equal to 0.027 and 0.016, respectively, at $R = 0.95$ and spacing between the plates of 4 mm. There are several reasons that actual spectral resolution is lower than the calculated one. Those may be as follows.

1. Working mirror surfaces are not parallel. For plates used the deviation (according to their certificate) did not exceed 0.004 of an interference fringe in the region of 0.25 μm. This can result in line blurring to 0.08 of the interferometer free spectral range.

2. Granular structure of a photoemulsion and a finite width of a recording microphotometer slit.

3. Self-broadening of the line emitted by a mercury lamp used.

4. Gas temperature in the glow discharge.

5. Magnetic field inhomogeneity when studying Zeeman effect.

6. Other processes in the glow discharge.

The isotopic mercury composition may be considered constant to a high degree of accuracy. Investigations of the natural isotopic fractions of mercury[10–12] allow one to estimate (usually relative to ^{198}Hg isotope) a change of relative isotope content to be below one thousandth. Several researchers have studied the mercury isotopic composition inside meteorites. In some investigations the deviation from standard terrestrial ratio was observed to be 20% as much. However, the deviations observed in these same samples that do not exceed 1% in the majority of cases are most likely true to life.

3. DOPPLER HALF-WIDTH OF THE MERCURY EMISSION LINE AT $\lambda = 254$ nm

At present, the line shapes of isolated absorption lines broadened due to Doppler effect have been studied experimentally in many gases. In all cases the measured half-widths coincide with those calculated by known formula (1) to a high accuracy[13]:

$$\gamma_D = 3.58 \cdot 10^{-7} \nu_0 (T/m)^{1/2}, \quad (1)$$

where γ_D is the profile half-width in cm^{-1}, ν_0 is line center frequency in cm^{-1}, T is the gas temperature in K, m is the atomic mass. In our experiment we had the following values: $T = 293$ K, $\nu_0 = 39417$ cm^{-1}, $m = 200.5$, and $\gamma_D = 0.0171$ cm^{-1}.

The emission line has the Doppler profile whose width can vary from 0.07 to 0.137 cm^{-1} and even broader. This broadening is much wider than the calculated Doppler one what could be associated with the processes in the glow discharge.[14,15] Figure 6 presents an interferogram obtained in our experiments that shows the isotopic structure of the line. This line was emitted by a VSB–1 capillary lamp filled with the natural mixture of mercury isotopes. Figure 7 shows an interferogram of the line emitted by a capillary high-frequency electrodeless lamp of VSB–1 type filled with the natural isotope mixture, Ar as a broadening gas at 2.5 mm Hg pressure and 40°C temperature. To avoid the line self-reversal, we used 1-mm-thick capillary lamp because the line emitted by a 10-mm-diameter bulb is strongly self-reversed to resolve the isotopic components. The absence of self-reversal when line is emitted by a capillary lamp has been checked up experimentally. In our experiments we also obtained the emission line whose width exceeded the calculated Doppler width of the absorption line. We used a Fabry-Perot interferometer with the instrumental function about 0.002 cm^{-1} wide. The close values for the width were obtained by the magnetic scanning method (Fig. 8), where the instrumental function is the line profile of emission from a monoisotope lamp that was used when recording Doppler contour of the absorption line.

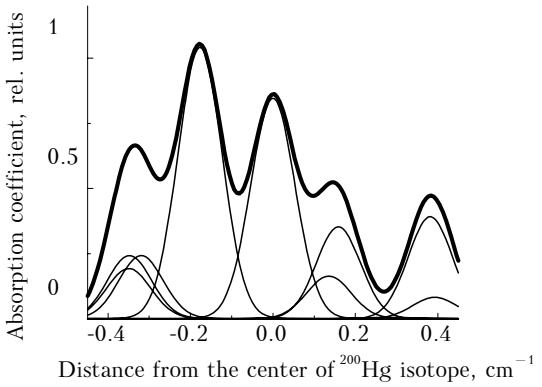

FIG. 6. Isotopic composition of natural isotope mixture. Doppler line profiles have the width obtained from our interferograms. Bold solid line is the integrated spectrum. Interferometer instrumental function width is 0.02 cm^{-1}.

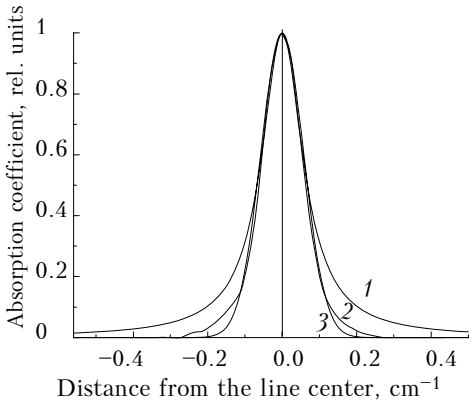

FIG. 7. Line profiles brought into coincidence on width and height: the Lorentz profile (1), the interferogram of the monoisotope line radiation recorded in our experiments (2), Doppler profile (3).

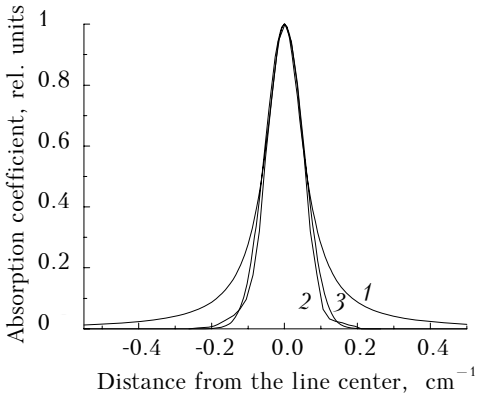

FIG. 8. Line profiles brought into coincidence on width and height: the Lorentz profile (1), the interferogram of the monoisotope line radiation recorded by the magnetic scanning method (2), Doppler profile (3).

When using a magnetic scanning method the source is a monoisotope lamp placed in the longitudinal magnetic field. When working with mercury, this lamp is filled with an even isotope to avoid the effects of hyperfine structure. In this case the lamp emits two spectral components along the magnetic field lines, with the frequency shifts of these components from the unshifted line center being proportional to the magnetic induction. A quarter-wave plate and a linear polarizer are used to separate out one σ component of the emission. Next are the cell with mercury vapor under the study and a photodetector. There is a version when the cell is placed into the magnetic field instead of the emitter. The spectral resolution is, in this case, determined by the emission (absorption) line width of the Zeeman component. This width, in its turn, depends on pressure and temperature in the cell or in the lamp. Besides, the emission line width depends on the self-reversal effect that leads to line broadening. The Zeeman component shift in the magnetic field is proportional to the magnetic induction value. The position of hyperfine structure components is usually determined relative to one of them, more often it is the line of ^{200}Hg isotope. It should be noted that the positions of the hyperfine and the isotopic composition components are well known,[1,3,4] so magnetic scanning is mostly used to control the mercury isotopic composition.[16] The magnetic scanning method is simpler and less expensive than the neutron activation analysis and mass-spectrometry method that are used most often. Together with our colleagues from St.-Petersburg University we have proposed a method for detecting variations in the isotope composition of mercury that is a further development of the magnetic scanning method.[17]

4. COLLISIONAL BROADENING AND SHIFT OF THE 254-NM MERCURY LINE

The Lorentz line profile width and the shift of its center are proportional to a broadening gas pressure in a wide pressure range.[1] The experimental data on broadening of the 254-nm mercury line by nitrogen, carbon dioxide, argon, and hydrogen obtained in Ref. 1 in the pressure range from 0 to 50 atm well confirm this fact. The broadening and shift coefficients for the 254-nm mercury line were published in Ref. 18. Table II presents data from Refs. 1 and 18 brought into a comparable scale. Taking into account these data as well as the results of isotopic composition determination obtained by authors of this paper and other researchers, we have constructed the integrated profile of the 254-nm mercury line at atmospheric pressure (see Fig. 9).

TABLE II. Broadening and shift coefficients of the 254-nm *mercury line by different gases.*

Broadening gas	Broadening coefficient, cm^{-1}/atm	Shift coefficient, cm^{-1}/atm	Ref.
He	0.236	+0.0129	18
Ne	0.151	−0.0225	−"−
Ar	0.312	−0.0699	−"−
Kr	0.209	−0.0538	−"−
Xe	0.301	−0.0673	−"−
N_2	0.149	−0.118	1
CO_2	0.232	−0.103	−"−
Ar	0.164	–	−"−
H_2	0.204	−0.0653	−"−

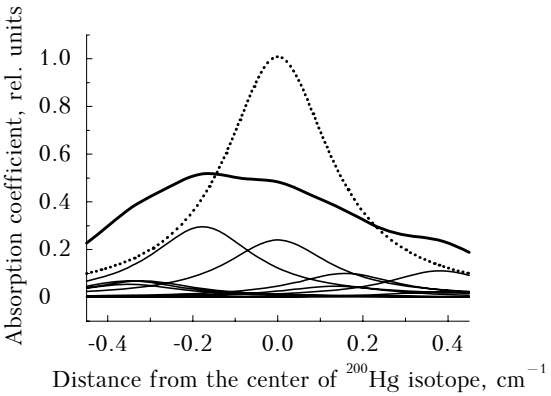

FIG. 9. Profiles of the 254-nm *absorption line at P* = 1 atm *(air as the broadening gas) for monoisotope mercury (dashed line) and natural isotope mixture (bold solid line). Thin lines are the profiles of the absorption lines for the isotope components accounting to their relative concentration in the natural mixture. Absorption coefficient at the center of the monoisotope line under normal conditions was taken as a unit.*

5. MEASUREMENTS OF ABSORPTION CROSS-SECTION OF MERCURY VAPOR AT 254-nm WAVELENGTH

Although this line is very well studied, the values of absorption cross-sections presented in different

papers[19,20] are considerably different. This may result from distinctions in spectral characteristics of both emission sources used and samples studied. The isotopic composition, line broadening and pressure shift, the source and sample temperature, and so on, should certainly influence the source and sample spectral characteristics.

When developing the mercury gas analyzer RGA–11 intended for quantitative measurements of a mercury content in different media,[21] we had to determine the exact value of the absorption cross-sections for the conditions wherein the measurements of mercury content ought to be carried out. At the first sight this work seems to be unnecessary because there are standard samples for acquiring the calibration data. Our experience showed that mercury content in these samples may vary by several times and, moreover, it changes with time.[22] So we have carried out direct measurements of the absorption cross-sections by the spectrophotometric method using mercury lamps of two types.

We used a set of quartz cells having different thickness. These cells were filled with saturated mercury vapor of natural isotopic composition and air added to make the atmospheric pressure in the cell at room temperature. The cell thicknesses were 0.6, 1.2, and 2.4 mm, respectively.

A DB4 lamp with natural isotope mixture and a high-frequency electrodeless monoisotope VSB–1 (^{204}Hg) lamps were used as the emission sources. The VSB–1 lamp was used in two versions: without magnetic field and in longitudinal magnetic field with 0.42 Tl induction.

It was of certain interest to compare the experimental ratio between the cell transmissions for the split and nonsplit line with the calculated value of this ratio. We have also estimated the transmission for radiation from a source with natural isotopic mixture because such sources are used in simple atomic absorption analyzers (like, for example, YULIYA and AGP–01).

We used a YULIYA–2M mercury analyzer in the experimental setup. A DB4 lamp was the emitter and a F28 was photocell photodetector. The cells with saturated mercury vapor and other attenuators were placed instead of YULIYA's analytic cell. The VSB–1 lamp radiation was directed to the photocell by means of a long-focus lens and through the same attenuators without changing the analyzer design.

The intensity of radiation from the sources was read out from YULIYA's digital indicator. Before measurements, the intensities were equalized by changing the distance between the VSB–1 lamp and the photocell. The cell transmission was determined as the ratio between the indicator readings with and without the cell. The attenuation of source radiation by cell windows has been taken into account by measuring the transmission of a cell that has no mercury vapor inside but having the same windows as the cells with mercury vapor. The linearity of the receiving and amplifying channel was controlled by placing attenuators with known transmission of 30 and 90% in the beam path.

The absorption cross-section value was determined from the following formula:

$$Q = -\ln T/nl, \qquad (2)$$

where T is the transmission measured, l is the thickness of the cell with saturated mercury vapor, n is the concentration of the saturated mercury vapor atoms at a temperature of 23.4°C.

6. PHOTOMETRY ERRORS

The single pass scheme of YULIYA analyzer provides an accuracy of 1% when measuring the transmission because the measurement with the cell takes one minute while during the rest time 100% transmission is recorded (intensity of the source radiation is measured). The latter signal is constant accurate to the last digit on YULIYA's indicator.

The cells were not thermostated and their temperature was thought to be equal to the room temperature. The cells were thermally insulated from the analyzer's frame that is warmer by means of insulating pad. Figure 10 shows the correcting effect of this pad.

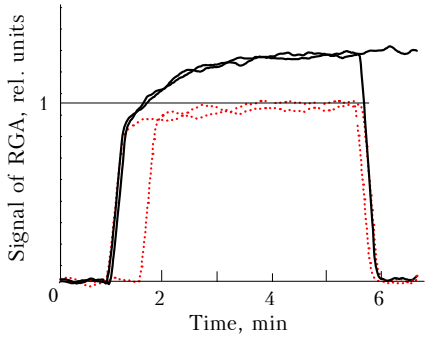

FIG. 10. Influence of calibration cell heating on the RGA-11 analyzer signal. Lower curves are for the case when there is a heat-shielding pad, upper ones – without a pad. Room temperature is 19.3°C, *analyzer's frame temperature is* 23.4°C. *Cell thickness is* 200.5 μm.

We have carried out five measurements for each cell and that yielded the rms measurement error of 6%. We did not carry out detailed measurements because our task was to estimate the range of mercury concentrations where linear approximation of the Bouguer law holds.

There is no way to calculate spectral values of the absorption cross-sections of mercury atom based only on fundamental constants. The direct measurements allow one to achieve the accuracy of 1%. Besides, we estimated the error due to nonmonochromaticity of radiation used in the magnetic scanning method (the

radiation nonmonochromaticity + the width of the interferometer instrumental function). Calculations showed that even at the strongest nonmonochromaticity of radiation we had in the experiment, the extra error did not exceed 3.5% (see Fig. 11). In real analytical measurements an optical thickness, τ, does not exceed 0.1, therefore the influence of the instrumental function can be neglected.

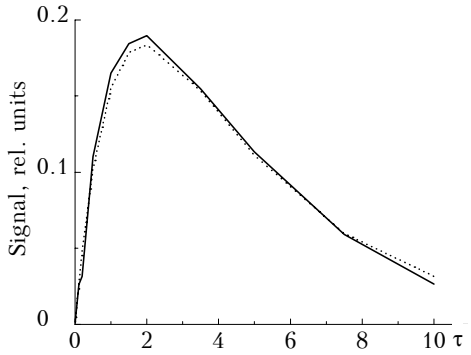

FIG. 11. Dependence of the differential signal value on optical thickness at the natural isotope mixture profile center. Broadening by atmospheric air under normal conditions. Solid line corresponds to the monochromatic radiation, dashed one to the Zeeman components having Doppler profile with the half-width of 0.063 cm^{-1}*, as in our experiment.*

7. QUANTITATIVE CHARACTERISTICS OF THE 254-NM MERCURY ABSORPTION LINE

1. The isotopic and hyperfine structure widths are the following: $\Delta\nu = 0.743$ cm^{-1}, $\Delta\lambda = 0.005$ nm.

2. Figure 1 presents the distances between spectral components of the isotopic and hyperfine structures.

3. Absorption cross-sections are the following:

$^{204}Q = 2.52 \cdot 10^{-14}$ cm^2 is the absorption cross-section when mercury vapor of natural isotope mixture absorbs the ^{204}Hg monoisotope lamp emission under normal conditions (air as the broadening gas). This corresponds to $Q = 5.25 \cdot 10^{-14}$ cm^2 which is absorption cross-section at line centers of the even isotopes that have no hyperfine structure (according to data from Ref. 18 $Q = 5.6 \cdot 10^{-14}$ cm^2).

$Q_{nat} = 2.73 \cdot 10^{-14}$ cm^2 is the absorption cross-section at the maximum of the integrated line profile of natural isotope mixture (air as the broadening gas, see Fig. 9).

$(^{204}Q_{\sigma-} + {}^{204}Q_{\sigma+})/2 = 1.56 \cdot 10^{-14}$ cm^2 is the mean absorption cross-section for σ-components of ^{204}Hg monoisotope line at $B = 0.42$ Tl.

$Q_{dif} = 1.51 \cdot 10^{-14}$ cm^2 is the differential absorption cross-section for the same conditions.

4. The 254-nm absorption line intensity $I = 7 \cdot 10^{-15}$ cm (considering that isotopic composition change does not influence the intensity).

5. Doppler width of the monoisotope absorption line under normal conditions is 0.034 cm^{-1}.

6. Monoisotope radiation line width obtained in the experiments (interferogram, magnetic scanning at broadening gas pressure from 1 to 2.5 mm Hg) is from 0.088 to 0.125 cm^{-1} (see Fig. 6).

7. Collisional broadening and shift coefficients are presented in Table I.

8. Zeeman splitting obtained in our experiments by means of constant magnet and the above-described interferometer is the distance between σ-components $\Delta\nu_z = 1.40$ cm^{-1}/Tl, the experimental value of the Lande factor is 1.49, while the calculated one is 1.5.

8. METROLOGICAL APPENDICES

The results of this paper we used to improve the techniques for mercury concentration determination by atomic absorption method without the use of calibration standards.

The problem of mercury analyzers' calibration lies in the fact that due to mercury sorption properties it is impossible to make a stable mercury concentration in a closed volume. Nowadays the following techniques for analyzers' calibration in air have been certified and used:

1. Dynamic dosing (continuous mercury vapor diffusion into the carrier-gas flux that passes through an analytic cell). Diffusion occurs from a thermostated vessel containing metallic mercury through a capillary or porous membrane.

2. Pulsed dosing (pulsed injection of mercury microquantities into the carrier-gas flux). A portion of mercury vapor is taken by syringe from a vessel containing saturated mercury vapor.

3. Thermal mercury sublimation from powder of a standard sample.

These methods have a number of disadvantages, these are instability of sorbent parameters, manual procedure when using a saturated mercury vapor, that leads to an increase in the influence of subjective factors on measurement results, volume inhomogeneity, and uncontrollable mercury content changes in standard samples when stored, cumbersome procedures, etc.

Analysis of mercury analyzers' calibration techniques (a separate paper will be devoted to this study) showed that use of physically equivalent techniques based on the absorption of 254-nm resonance line by saturated mercury vapor would allow one to overcome these disadvantages. Thin cells with saturated mercury vapor are those physical equivalents in our study. The saturated mercury vapor concentration in the cells is kept constant due to the evaporation from a mercury drop surface. Such a drop is placed between quartz windows separated by a Teflon pad of a known thickness. The thickness of such a cell varies from tens to hundred microns. The measurement accuracy of the cell length (thickness) is on the order of tenth of a micron and

the windows are parallel accurate to seconds of arc. The temperature of the cell determines the saturated vapor pressure. Figure 12 shows the dependence of saturated mercury vapor pressure on temperature as well as of the signal from an RGA–11 analyzer under varying temperature of the cell. The mercury purity and the drop diameter do not influence the results. Table III summarizes the results of certification of the cells' thickness carried for several years at D.I. Mendeleev All-Union Scientific-Research Institute for the same set of cells. The certification has been carried out by comparing the signals from cells under control and the cell through which vapor from standard mercury vapor generator was blown.

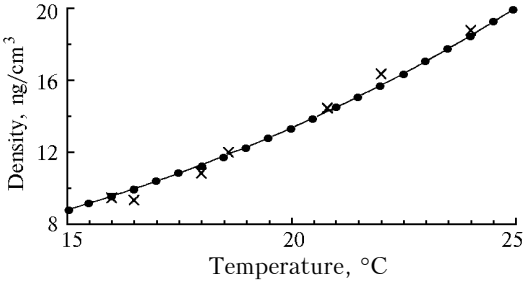

FIG. 12. Dependence of saturated mercury vapor density on temperature over a temperature range corresponding to calibration technique. Crosses are the RGA-11 readings, dots are the table data, and solid line is calculation by an empirical formula.

TABLE III. Cells' thicknesses certified by Tomsk Center of Standard and Metrology (this set of cells is used during 5 years). Certification was carried out on the standard analyzer with the standard cells certified at D.I. Mendeleev All-Union Scientific-Research Institute. No certification was done in 1993.

Cell number	Certified thickness, μm					Average value,	Rms deviation	
	1992	1994	1995	1996	1997	μm	μm	%
1	38	43	38	45	43	41	2.9	7.0
2	106	111	95	108	106	105	5.4	5.1
3	191	194	195	188	191	192	2.5	1.3
4	574	536	585	577	566	568	16.9	2.3

The difference in the thickness measured just after manufacturing and in a year does not exceed 5%.

9. ESTIMATION OF POTENTIALITIES OF LASER SENSING OF MERCURY

Estimations of mercury laser sensing potentialities were made at Scientific-Research Institute of the Earth Crust. Recently a portable mercury lidar has been used for geothermal areas mapping.[23,24] The surveys have shown that such devices are very useful because they can control not only large areas but also measure pollutions from a separate source.[25] Implementation of a refined quantitative spectral characteristics of the 254-nm mercury emission line will allow one to essentially improve results of laser sensing of atmospheric mercury.

The authors are grateful to Dr. L.A. Konopel'ko and Dr. Yu.N. Ponomarev for useful discussions which stimulated this paper publication.

REFERENCES

1. S.E. Frish, *Optical Spectra of Atoms* (Fizmatgiz, Moscow, 1963).
2. M.A. El'yashevich, *Atomic and Molecular Spectroscopy* (Fizmatgiz, Moscow-Leningrad, 1962).
3. J. Chem. Phys. **21**, 1762 (1952).
4. L. Bradley, Proc. Roy. Soc. **262**, 1308 (1961).
5. A.N. Zaidel', *Basis of Spectral Analysis* (Nauka, Moscow, 1965), 324 pp.
6. O. Vasiliev, A. Kotkin, D. Stolyarov, et al., Trudy Latv. Univ. **573**, 105–110 (1992).
7. Diffraction Spectrograph DFS-452, Passport G34.19.051 PS (1976).
8. V.V. Lebedeva, *Instrumentation for Optical Spectroscopy* (State University, Moscow, 1977), 384 pp.
9. V.I. Malyshev, *Introduction into Experimental Spectroscopy* (Nauka, Moscow, 1979), 479 pp.
10. A.A. Obolenskii and E.F. Doil'nitsyn, Dokl. Akad. Nauk SSSR **230**, No. 3, 701–704 (1976).
11. V.V. Kuznetsov and A.A. Obolenskii, Dokl. Akad. Nauk SSSR **252**, No. 2, 459–460 (1980).
12. A.A. Obolenskii, *Genesis of Mercury Ore Deposits* (Nauka, Novosibirsk, 1985).
13. A.B. Antipov, V.A. Kapitanov, Yu.N. Ponomarev, and V.A. Sapozhnikova, *Photo-Acoustic Method in Laser Spectroscopy of Atmospheric Gases* (Nauka, Novosibirsk, 1984), 128 pp.
14. A. Skudra and V. Khutorshchikov, Trudy Latv. Univ. **573**, 4–28 (1992).
15. S.V. Semyonov and N.N. Yakobson, Vopr. Radioelektron., Ser. Opt. Tekh., Issue 6, 138–143 (1968).
16. N.R. Stankov, "*Production of high-enriched mercury isotopes by photochemical method*,B Cand. Phys.-Math. Sci. Dissert., Moscow (1993).
17. A.A. Ganeev, S.E. Sholupov, A.B. Antipov, and A.D. Maidurov, "*Method of differential absorption isotope analysis*,B Inventor's Certificate No. 1805356, October 9, 1992.
18. F. Schuller and W. Behmenburg, Physics Reports (Section of Physics Letters) **12**, No. 4, 273–334 (1974).
19. Byer, Opt. Quantum Electron. **7**, 147–177(1975).
20. *Investigations of analytical characteristics of the atomic absorption Zeeman analyzer for aerogeochemical survey from the gaseous mercury halos*, Report on the contract No. 366/75, Leningrad (1985).
21. A.B. Antipov, E.Yu. Genina, N.G. Mel'nikov, and G.V. Kashkan, Atmos. Oceanic Opt. **7**, Nos. 11–12, 886–889 (1994).
22. A.B. Antipov, E.Yu. Genina, N.G. Mel'nikov, G.V. Kashkan, and N.A. Ozerova, Chemistry for Sustainable Development (1998) (to be published).

23. H. Edner, G.W. Faris, A.Sunesson, and S. Svanberg, Appl. Opt. **28**, 921–930(1989).
24. H. Edner, P. Ragnarson, S. Svanberg, E. Wallinder, et al., J. Geophys. Res. **97**, 3779–3786 (1992).
25. M. Horvat, *NATO ASI Series 2: Environment. Global and Regional Mercury Cycles: Sources, and Mass Balances* (Kluwer Academic Publishers, Dordrecht, Boston, London, 1996).